JGR Space Physics

RESEARCH ARTICLE
10.1029/2019JA027077

Expansion and Shrinking of the Martian Topside Ionosphere

E. Dubinin[1], M. Fraenz[1], M. Pätzold[2], J. Woch[1], J. McFadden[3], J. S. Halekas[4], J. E. P. Connerney[5], B. M. Jakosky[6], F. Eparvier[6], O. Vaisberg[7], and L. Zelenyi[7]

[1]Max-Planck-Institute for Solar System Research, Göttingen, Germany, [2]Rheinisches Institut fuer Umweltforschung, Abteilung Planetforschung, Cologne, Germany, Space Sciences Laboratory, U.C. Berkeley, Berkeley, CA, USA, [4]Department of Physics and Astronomy, University of Iowa, Iowa City, IA, USA, NASA Goddard Space Flight Center, Maryland, USA, Laboratory for Atmospheric and Space Physics,University of Colorado, Boulder, CO, USA, [7]Institute of Space Research, Moscow, Russia

Key Points:
- Upper ionosphere of Mars is very sensitive to the solar wind variations
- Upper ionosphere of Mars is very sensitive to the variations of the interplanetary magnetic field
- Upper ionosphere of Mars is very sensitive to the planetary crustal field

Correspondence to:
E. Dubinin,
dubinin@mps.mpg.de

Citation:
Dubinin, E., Fraenz, M., Pätzold, M., Woch, J., McFadden, J., Halekas, J. S., et al. (2019). Expansion and shrinking of the martian topside ionosphere. *Journal of Geophysical Research: Space Physics*, *124*, 9725–9738. https://doi.org/10.1029/2019JA027077

Received 27 JUN 2019
Accepted 13 OCT 2019
Accepted article online 9 NOV 2019
Published online 30 NOV 2019

Abstract The observations made by the Mars Atmosphere and Volatile EvolutioN spacecraft in the topside (≥200 km) ionosphere of Mars show that this region is very responsive to the variations of the external (solar extreme ultraviolet flux, solar wind, and interplanetary magnetic field [IMF]) and internal (the crustal magnetic field) drivers. With the growth of the solar irradiance the ionosphere broadens while with increase of the solar wind dynamic pressure it shrinks. As a result, the upper ionospheric boundary at solar zenith angles of 60–70° can move from ~400 to ~1,200 km. Similar trends are observed at the nightside ionosphere. At $P_{dyn} \geq$ 1–2 nPa the nightside ionosphere becomes very fragmented and depleted. On the other hand, the ion density in the nightside ionosphere significantly (up to a factor of 10) increases with the rise of the solar extreme ultraviolet flux. Large-amplitude motions of the topside ionosphere also occur with variations of the value of the cross-flow component of the IMF. The upper dayside ionosphere at altitudes of more than 300–400 km is sensitive also to the direction of the cross-flow component of the IMF or, correspondingly, to the direction of the motional electric field in the solar wind. The ionosphere becomes very asymmetrical with respect to the $V_{sw} \times B_{IMF}$ direction and the asymmetry strongly enhances at the nightside. The topside ionosphere above the areas with strong crustal magnetic field in the dayside southern hemisphere is significantly denser and expands to higher altitudes as compared to the ionosphere above the northern nonmagnetized lowlands. The crustal magnetic field also protects the nightside ionosphere from being filled by plasma transported from the dayside. The draping IMF penetrates deeply into the ionosphere and actively influences its structure. Weak fields and, correspondingly, weak magnetic field forces only slightly affect the ionosphere. With increase of the induced magnetic field strength the transport motions driven by the magnetic field pressure and field tensions seem to be intensified and we observe that the local ion densities at the dayside considerably decrease. A different trend is observed at the nightside. The ion density in the nightside ionosphere above the northern lowlands is higher than in the southern hemisphere indicating that plasma transport from the dayside is the main source of the nightside ionosphere. Nonstop variations in the solar wind, the IMF and the solar irradiance together with planetary rotation of the crustal magnetic field sources lead to a continuous expansion/shrinking and reconfiguration of the topside ionosphere of Mars.

1. Introduction

The Martian ionosphere was first detected by the Mariner-4 spacecraft Kliore et al., 1965 and then extensively sampled by the radio occultation, radar sounding, and in situ methods on other space missions (Hanson et al., 1977; Hinson et al., 1999; Kliore et al., 1992; Gurnett et al., 2005; Pätzold et al., 2005, 2016; Ergun et al., 2015). The bulk of the ionosphere at Mars is formed by solar extreme ultraviolet (EUV) (10–95 nm) photoionization of the major atmospheric neutrals (CO_2) followed by the photochemical production of O_2^+ ions (see, e.g., Schunk & Nagy, 2009 and Fox et al., 2017). A balance between photoionization and recombination (photochemical equilibrium) forms the peak electron density at altitudes between 120 and 150 km, depending on the solar zenith angle (SZA). The electron density in the peak and the SZA dependence are in a reasonable agreement with the Chapman model. The direct photoionization of oxygen atoms produced by photolysis of CO_2 together with the dissociative ionization of CO_2 generate a population of O^+ ions with

the density gradually increasing upwards to ~200–250 km. In addition to the main ionospheric peak, the lower-altitude layer between 90 and 130 km altitude is created by solar X-rays (≤10 nm) (Fox, 2004; Mendillo et al., 2006; Pätzold et al., 2016; Peter et al., 2014). Additional plasma is occasionally present between 70 and 110 km altitude. At $h \geq \sim 200$ km the ionosphere is no longer in photochemical equilibrium and diffusion and transport processes become dominant.

Variations in the ionosphere near the main peak are directly linked to the variability in the solar radiation. These include long-term temporal variations caused by the changing heliocentric distance (~1.38–1.67 AU) and the planetary season, changes in the solar output related to the solar rotation (~27 day) (Mendillo et al., 2013; Venkateswara Rao et al., 2014; Withers & Mendillo, 2005), the solar cycle (~ 11 year) (Mendillo et al., 2013, 2016; Sanchez-Cano et al., 2015, 2016; Withers et al., 2015), solar flares (Gurnett et al., 2005, 2008; Mendillo et al., 2006). Various effects of the periodic solar EUV forcing are also clearly observed in numerical simulations (e.g., in the Mars-Global Ionosphere-Thermosphere Model (e.g., Bougher et al., 2014).

The ionosphere below the main peak varies due to changes in the neutral atmosphere, dust storms, and solar flares. Large variations in this portion of the ionosphere at different phases of the solar cycle were observed by Sanchez-Cano et al. (2016) using the radio-occultation measurements by the Mars Radio Science experiment (Pätzold et al., 2009; Peter et al., 2014). Analyzing variability of the main peak during the period of very low solar variability, Mendillo et al. (2017) have found that the residual variability of the electron number density is due to a change in density of the CO_2 molecules that are ionized to form the ionosphere. Long-term variations in solar EUV flux with the solar cycle generally well control the ionospheric structure at altitudes above the main peak but below ~250 km (Sanchez-Cano et al., 2016).

The vertical structure of the dayside ionosphere at $h \geq \sim 200$ km occurs much more variable and complex than previously thought, with distinct deviations from the Chapman model (Ergun et al., 2015; Pätzold et al., 2016; Kopf et al., 2008; Peter et al., 2014). Substantial variations in the number densities of all ion species (Benna et al., 2015; Bougher et al., 2015) are typical for the topside ionosphere. At these altitudes the collision frequency strongly decreases and the ionosphere being no longer in photochemical equilibrium becomes very dynamic. Plasma transport processes are dominant here making this portion of the ionosphere critically important for ion losses. Nightside ion densities also show a high variability changing by nearly 1 order of magnitude (Girazian et al., 2017).

Although the topside ionosphere is no longer in photochemical equilibrium, solar irradiance remains to be important. Solar wind is another important driver since the topside ionosphere is in a direct contact with it. Crustal magnetic fields (Açuna et al., 1999; Connerney et al., 2005) can strongly reduce the mobility of ions and electrons in the ionosphere making them less exposed to vertical and horizontal motions. In this paper we study the role of all these factors for variability of the topside ionosphere. Analysis is made on the base of the measurements performed by the Supra-Thermal And Thermal Ion Composition (STATIC) instrument (McFadden et al., 2015) onboard the Mars Atmosphere and Volatile EvolutioN (MAVEN) spacecraft. The measurements provide the first systematic in situ measurements of the ion number densities of the different ion species in the Martian ionosphere with in situ monitoring of the solar irradiance, solar wind, and the ionospheric magnetization. In contrast to the observations by the Neutral Gas and Ion Mass Spectrometer instrument (Benna et al., 2015) the ion densities can also be measured by STATIC for the parts of the ionosphere in which the ions are in motion.

2. Observations

The MAVEN spacecraft arrived at Mars in September 2014 to study the processes in the upper atmosphere/ionosphere and its interaction with solar wind and the consequent escape of atmospheric species to space Jakosky et al., 2015. MAVEN was inserted into an elliptical orbit with periapsis and apoapsis of 150 and 6,200 km, respectively, and with a period of 4.5 hr. It carries a complete instrument package measuring the input fluxes of solar wind and solar irradiance and monitor the response of the Martian atmosphere/exosphere and ionosphere. In this paper we discuss observations made by the STATIC instrument on MAVEN spacecraft from 1 November 2014 to 15 August 2017. The STATIC instrument mounted on the Actuated Payload Platform is used to study the escape of planetary ions. It measures energy spectra of ion fluxes in the range of 0.1 eV to 30 keV and the ion composition (McFadden et al., 2015). The instrument consists of a toroidal top hat electrostatic spectrometer with an electrostatic deflector at the entrance providing 360° × 90° field of view combined with a time-of-flight velocity analyzer resolving the major ion species

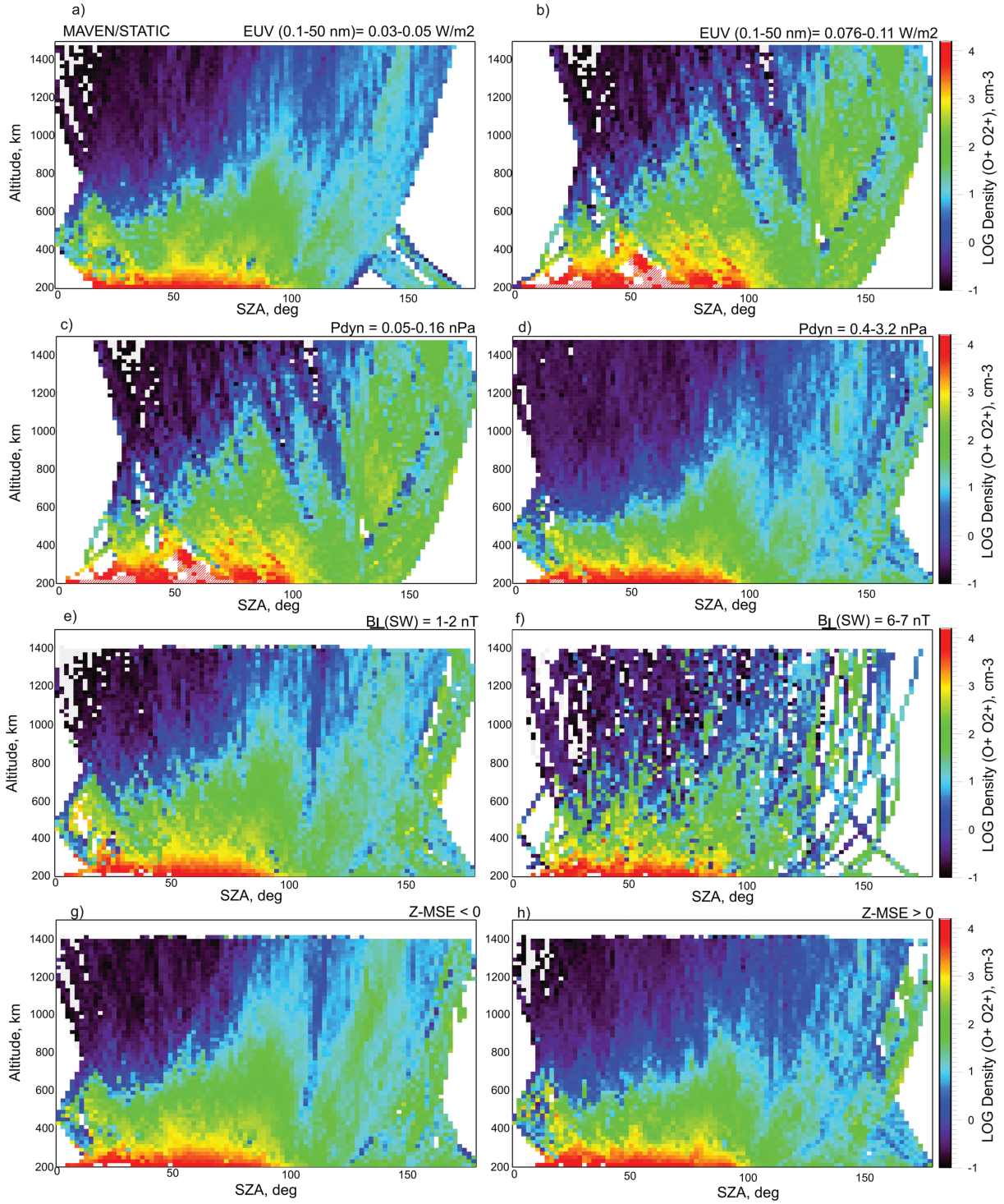

Figure 1. Maps of the median values of the oxygen ion number density in the SZA-altitude variables for different values of the solar irradiance (a, b); at two different levels of the solar wind dynamic pressure (c, d); at two different values of the cross-flow component of the IMF (e, f); and in two different MSE-hemispheres (g, h). Red shaded bins correspond to the densities with $LogN_i \geq 4.2$.

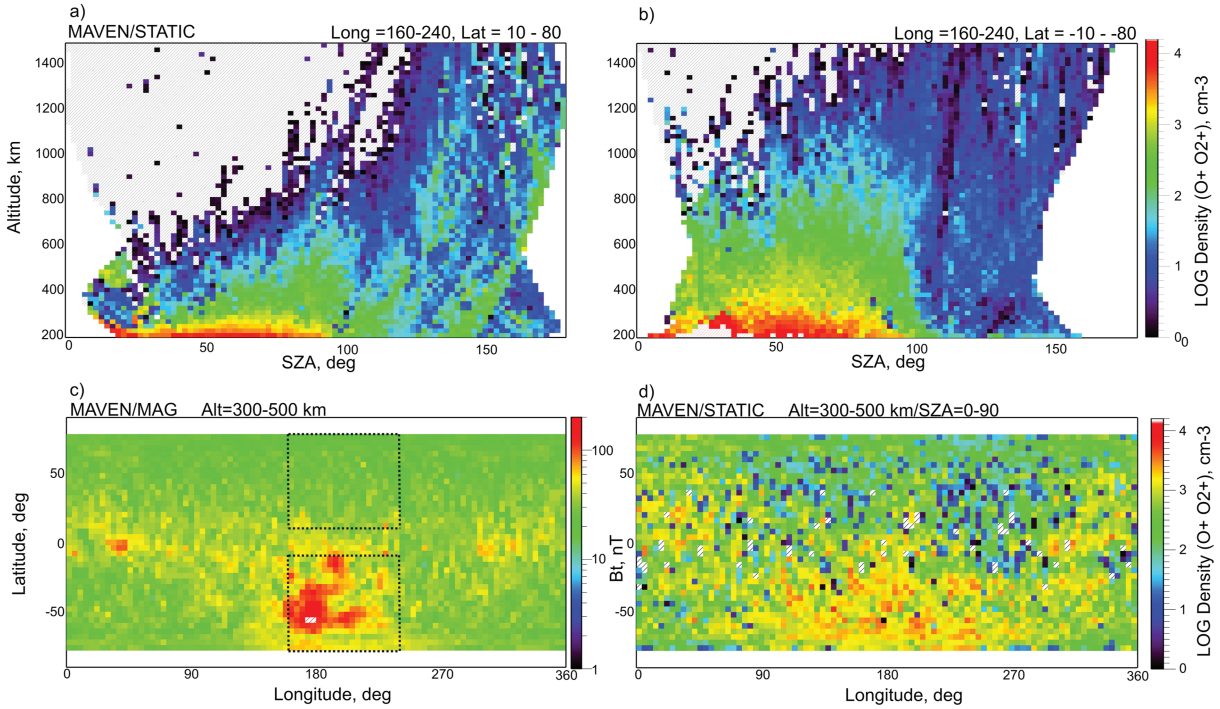

Figure 2. (a, b) SZA-altitude maps of n_i obtained in the northern and southern hemispheres for areographic longitudes 160–240°. (c) Map of the magnetic field strength in areographic coordinates at altitude of 300–500 km. Dotted lines bound the areas used for the maps shown in Figures 2a and 2b. (d) Map of the ion number density in areographic coordinates at altitude of 300–500 km.

H^+, He^{++}, He^+, O^+, O_2^+, and CO_2^+. The measurements allow a retrieval of the velocity distribution functions and their moments (density, velocity, and temperature) for different ion species. The measurements of the low-energy ions in the dense ionosphere and in the planetary wake are affected by the spacecraft potential. Therefore, calculating the ion distribution functions we made corrections using the spacecraft potential. Corrections related to the spacecraft velocity were also utilized. The instrument operates in different modes (RAM, Conic, and Pickup) providing different data products with different mass, energy, angular, and time resolution. In this study we used "joined" products which have 32 energy steps, 4 deflector angles (elevation angles), 16 anodes (azimuth angles), 8 ion masses, and 4 s cadence to calculate the moments of the ion distribution functions. Here we focus only on the observations of the number density of the oxygen ions (O^+ and O_2^+), which dominate in the topside ionosphere. The STATIC observations were complemented by EUV (Eparvier et al., 2015) and solar wind monitoring (Solar Wind Ion Analyzer; Halekas et al., 2015). The full EUV spectrum at Mars combining the MAVEN measurements and the observations at Earth orbit on

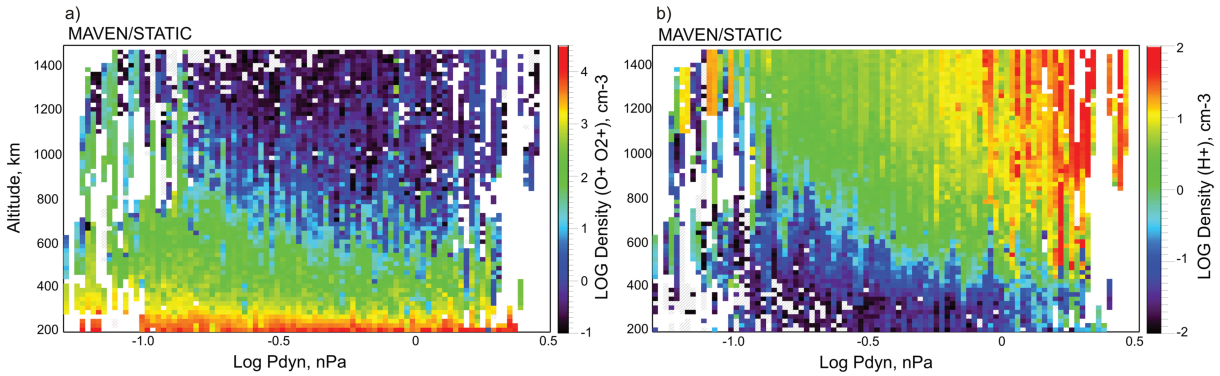

Figure 3. (a) Map of the oxygen ion number density in the ionosphere at SZA = 60–70° as a function of the solar wind dynamic pressure at different altitudes; (b) similar map for the protons with $E_e \geq 30$ eV. Black shaded bins in panels (a) and (b) correspond to the densities lower than 10^{-1} and 10^{-2} cm^3, respectively.

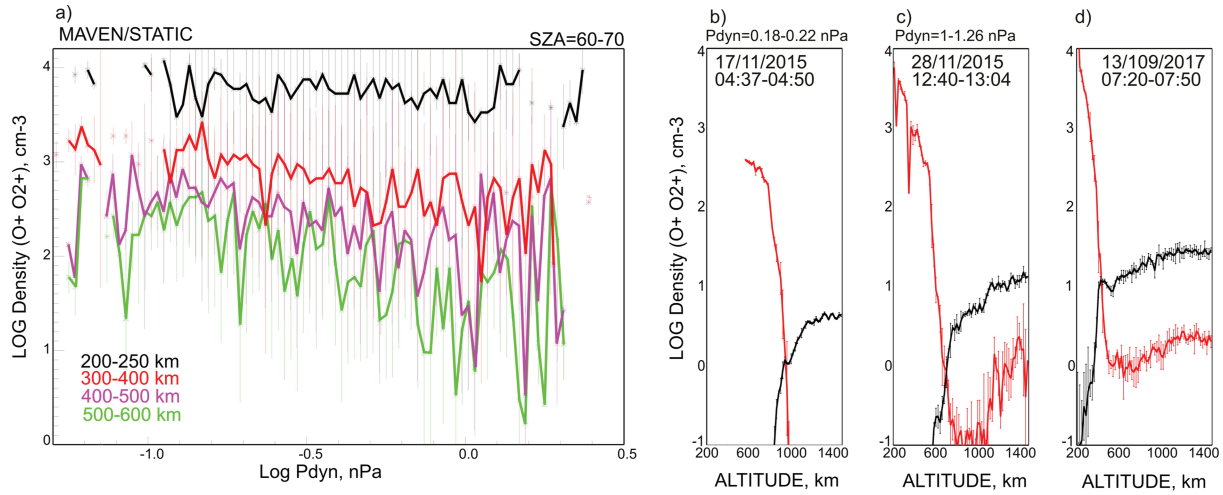

Figure 4. (a) Densities and their standard deviations of $(O^+ + O_2^+)$ ions at different altitudes as functions of the solar wind dynamic pressure. (b–d) Typical examples of the ion (oxygen = red and protons = black) density profiles obtained for three MAVEN orbits with different values of the dynamic pressure.

TIMED-SEE and SOLSTICE instruments interpolated to the Mars position at the time of the MAVEN measurements was provided (L3 data product) to characterize the EUV conditions at Mars. Monitoring of solar wind by Solar Wind Ion Analyzer is made with high cadence (4 s) measurements of ion velocity distributions in the 30 eV to 25 keV energy range with 14.5% energy resolution and 3.75° × 4.5° angular resolution in the sunward direction. The magnetic field measured by the magnetometer (Connerney, Espley, DiBraccio, et al., 2015; Connerney, Espley, Lawton, et al., 2015) was used to characterize the interplanetary magnetic field (IMF) and the ionospheric magnetization.

2.1. General Trends

There are several important processes controlling the density variations in the topside ionosphere. Solar radiation is probably the most important driver. Figures 1a and 1b compare maps of the median values of the total ion $(O^+ + O_2^+)$ number density in the SZA-altitude variables at two different levels of the solar irradiance (EUV). It is observed that the ion density at altitudes of ~200–300 km increases with a rise of the solar EUV flux. The ionosphere at higher solar irradiance also expands to higher altitudes that is well seen at SZA ≥60° and at the nightside.

Figures 1c and 1d compare maps of the median value of the oxygen ion number density in two different ranges of the solar wind dynamic pressure. Here we observe the opposite trend as compared to variations caused by EUV. At higher values of P_{dyn} the ionosphere shrinks and the ionospheric number density decreases at altitudes above 400–500 km. In contrast, at weak P_{dyn} the ionosphere expands upward.

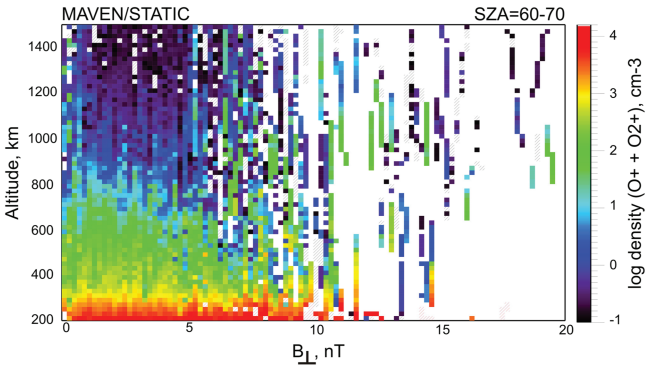

Figure 5. Map of the oxygen ion number density in the ionosphere at SZA = 60–70° as a function of the value of the cross-flow component of the IMF at different altitudes.

The topside ionosphere occurs to be responsive to the IMF. Figures 1e and 1f depict the ion density maps at different values of the cross-flow component of the magnetic field in the solar wind. At higher values of the $B_\perp$ the ionosphere shrinks and becomes more patchy at higher altitudes.

The ionosphere is also sensitive to the direction of the cross-flow component of the IMF and hence to the direction of the motional electric field in the solar wind $-v_{sw} \times B_{IMF}$. Figures 1g and 1h show SZA-altitude maps of the ion density in the different Mars Solar Electric (MSE) hemispheres, with $Z_{MSE} < 0$ and $Z_{MSE} > 0$, respectively. Note that in the MSE system the X_{MSE} axis coincides with the X_{MSO} axis, while the Y_{MSE} axis is determined by the magnetic field vector in the solar wind being along the cross-flow component of the IMF. Then the Z_{MSE} axis is always along the direction of the motional electric field $E_{sw} = -V_{sw}$ x B_{IMF}. To decrease a probable effect of the crustal magnetic field (see below), we exploited only the measurements carried out in the northern hemisphere where crustal fields are much weaker. It is observed that in the E^- hemisphere

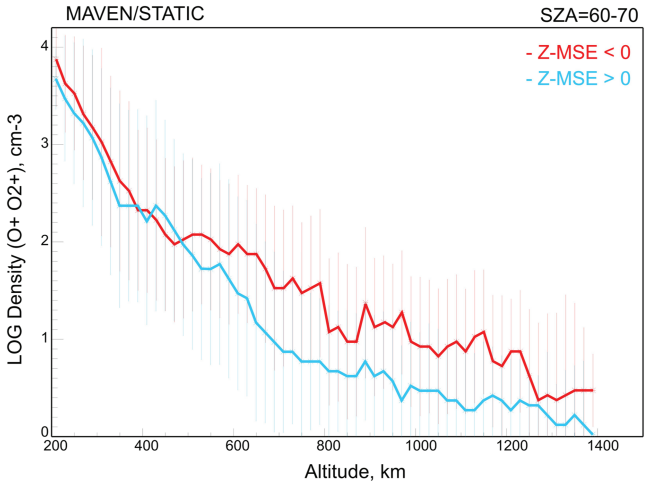

Figure 6. Altitude profiles of the median values and standard deviations of the ion ($O^+ + O_2^+$) number density measured in the E^- and E^+ hemispheres.

($Z_{MSE} < 0$) the ionosphere expands to higher altitudes than in the E^+ hemisphere ($Z_{MSE} > 0$) although the effect is weaker than for variations caused by the dynamic pressure.

Crustal magnetic fields also significantly influence the ionosphere structure by restricting the plasma transport there. Figures 2a and 2b compare SZA-altitude maps of the ion ($O^+ + O_2^+$) density measured in two parts of the northern and southern hemispheres for areographic longitudes 160–240° shown in Figure 2c by the dotted lines. The magnetic field conditions in these areas are very different. We observe that the ionosphere in the southern dayside hemisphere, which contains the strong crustal field sources, spreads to higher altitudes, and is generally denser as compared to the ionosphere in the northern hemisphere. On the other hand, when the southern regions with the strong crustal fields occur at the nightside the ionosphere is more depleted than at the north. An influence of the crustal field on the dayside ionosphere structure is also well seen in Figure 2d, which shows a map of n_i at 300-500 km altitude in areographic coordinates.

2.2. Dayside Ionosphere

Here we discuss in more detail how the topside ionosphere at SZA = 60–70° varies depending on the different parameters. The range of the SZAs is representative since it is close to the terminator that is the important region for the ion transport to the nightside and for ion losses (Fraenz et al., 2010, 2015). Figure 3a depicts a map of the ion ($O^+ + O_2^+$) density at SZA = 60–70° as a function of the solar wind dynamic pressure at different altitudes. It is observed that at low values of the dynamic pressure ($P_{dyn} \leq 0.1$ nPa) the ionosphere broadens up to 1,200-1,400 km and shrinks below ~500 km when the dynamic pressure increases up to ~2–3 nPa. A similar map for the protons with $E_i > 30$ eV (Figure 3b), which characterizes variations of the magnetosheath, verifies large-amplitude motions of the ionosphere in response to the solar wind variations. Figure 4a shows how the density at different altitudes changes with variations of the dynamic pressure. To exclude the influence of the solar irradiance only the measurements made at the EUV flux (0.1–50 nm) 0.04–0.05 W/m^2 were taken. We can see that the ionosphere is depleted with growing solar wind pressure. The effect is increasing with altitude h and even noticeable at $h \sim$ 200–250 km). It is worth noting that the averaged profiles in Figure 4a dilute the transition between the ionosphere and the magnetosheath that commonly is rather sharp. Figures 4b–4d depict typical examples of the profiles of the densities of the oxygen ions and the sheath protons near the upper boundary of the ionosphere measured at different values of the solar wind dynamic pressure. We also include the profile obtained during the impact of the September 2017 interplanetary coronal mass ejection (ICME). The shock related with the ICME arrived on 13 September at 02:52 UT (Lee et al., 2018). During the event MAVEN did not enter the solar wind and therefore there are uncertainties in the solar wind parameters. Results from the CME modeling provide the proxy peak values

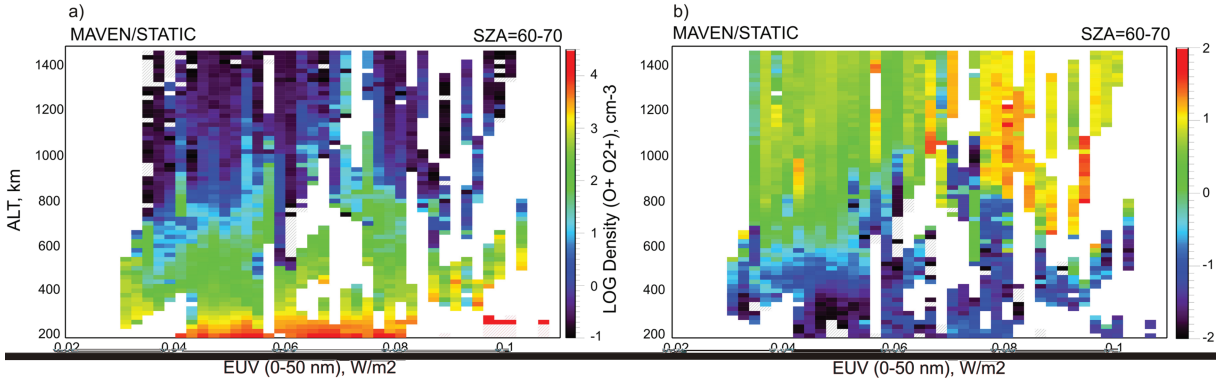

Figure 7. (a) Map of the oxygen ion number density at SZA = 60–70° as a function of altitude and the solar EUV flux (0.1–50‘nm); (b) map of the proton ($E \geq 30$ eV) number density.

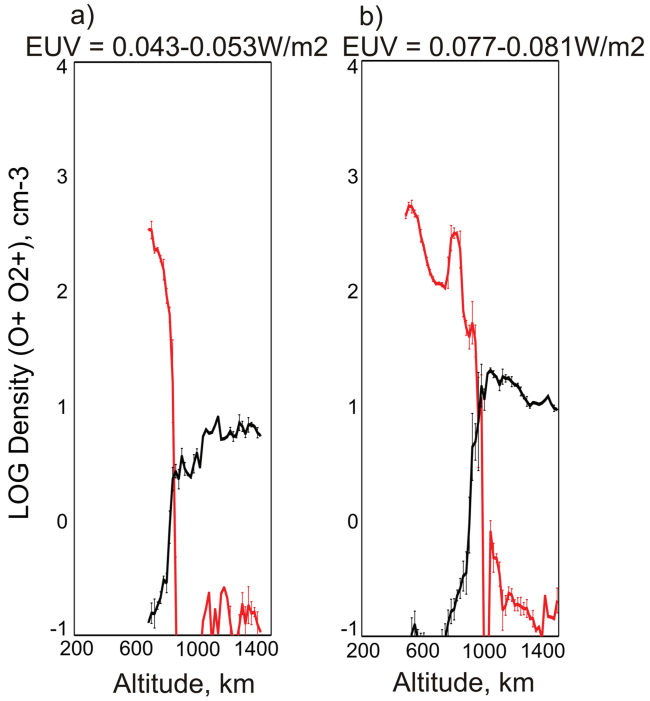

Figure 8. (a, b) Typical examples of the ion (oxygen = red and protons = black) density profiles obtained for two typical MAVEN orbits for the two ranges of the EUV flux.

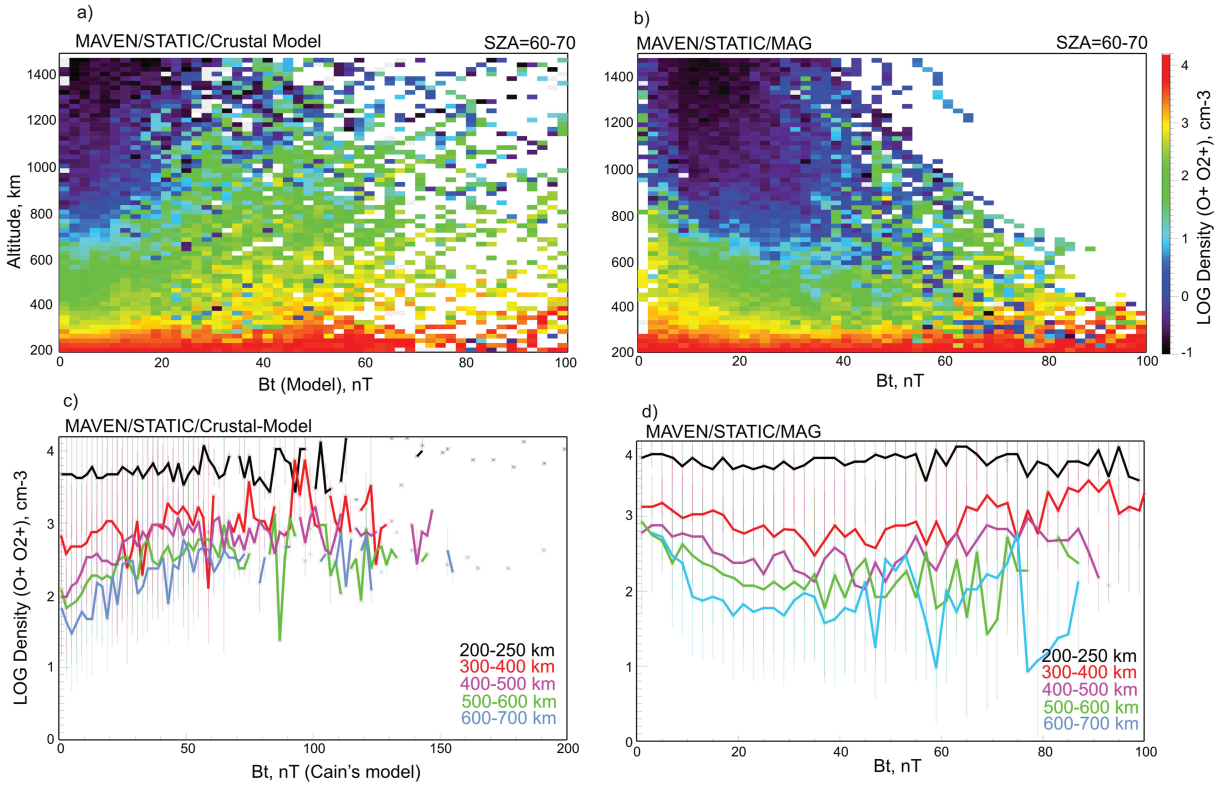

Figure 9. (a) Map of the ion ($O^+ + O_2^+$) number density at different altitudes at SZA = 60–70° as a function of the crustal magnetic field value from the Cain' model (Cain et al., 2003); (b) map of the ion ($O^+ + O_2^+$) density as a function of the in-situ measured magnetic field value; (c) relations between the ion density and the model magnetic field at different altitude intervals; (d) the same as in (c) but instead of the model value the actual in situ measured magnetic field strength is taken.

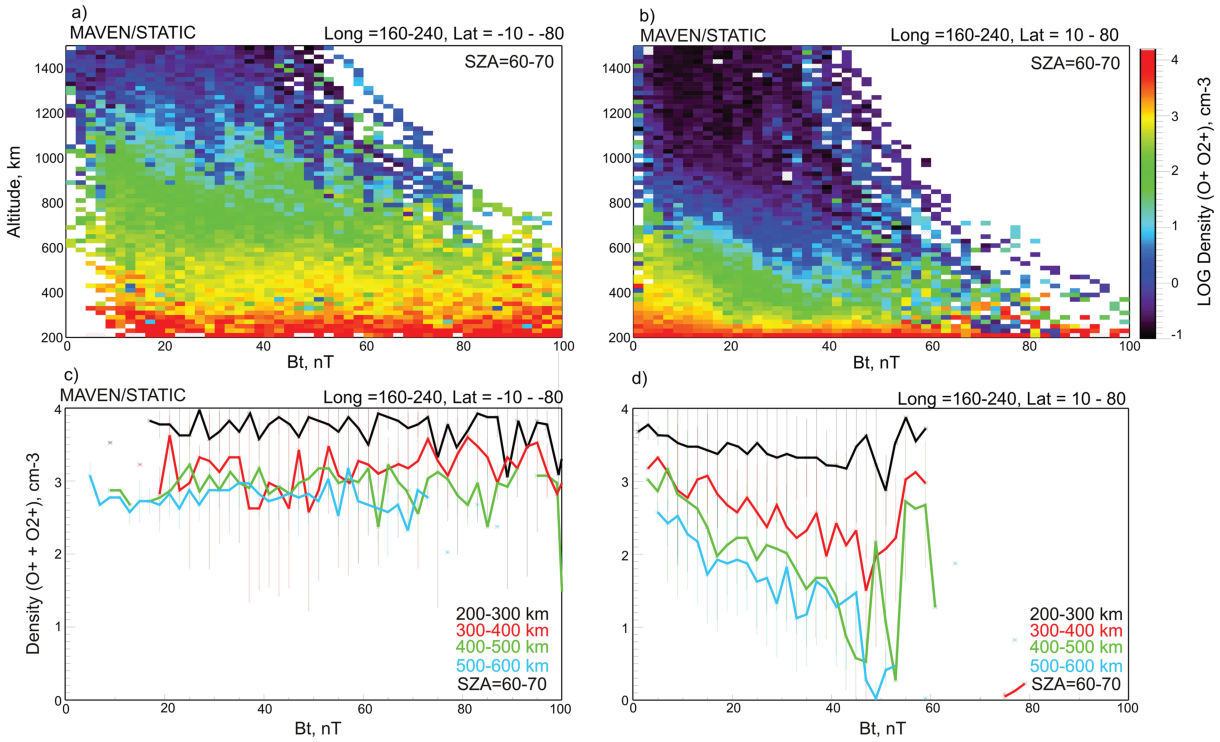

Figure 10. (a, b) Maps of the oxygen number density as a function of the magnetic field values in the ionospheric areas with strong and weak crustal fields, respectively (see Figure 2c). (c, d) Dependences of the ion density on the magnetic field value at different altitudes in the ionosphere with and without crustal field, respectively.

of the dynamic pressure in the range of 3.4–3.8 nPa. Ma et al. (2018) have inferred the parameters of the upstream solar wind by fitting the MAVEN observations in the magnetosheath to a MHD model. According to Ma et al. (2018) the peak value of the dynamic pressure reached 20.8 nPa at 8 UT. It is seen that the ionosphere contracts from ~1,000 to 600 km. with increase of the dynamic pressure from ~0.2 to ~1.2 nPa. During the ICME impact the ionosphere at SZA = 60 − 70° shrinks down to ~400 km. We do not observe a visible effect of compression at low altitudes implying that the upper portion of the ionosphere might be lost during strong pressure pulses. The observations of a sharp drop of the ionospheric density (ionopause) and its motions with the solar wind pressure are consistent with the PVO results on Venus (Phillips et al., 1985).

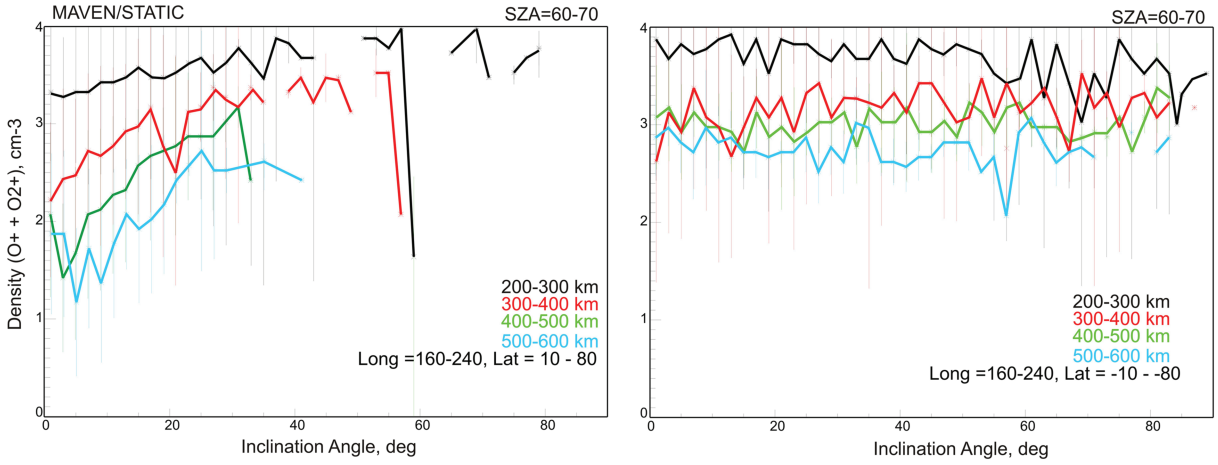

Figure 11. (a, b) Dependences of the ion density on the magnetic field geometry (the inclination angle) at different altitudes in the ionosphere without and with crustal fields, respectively.

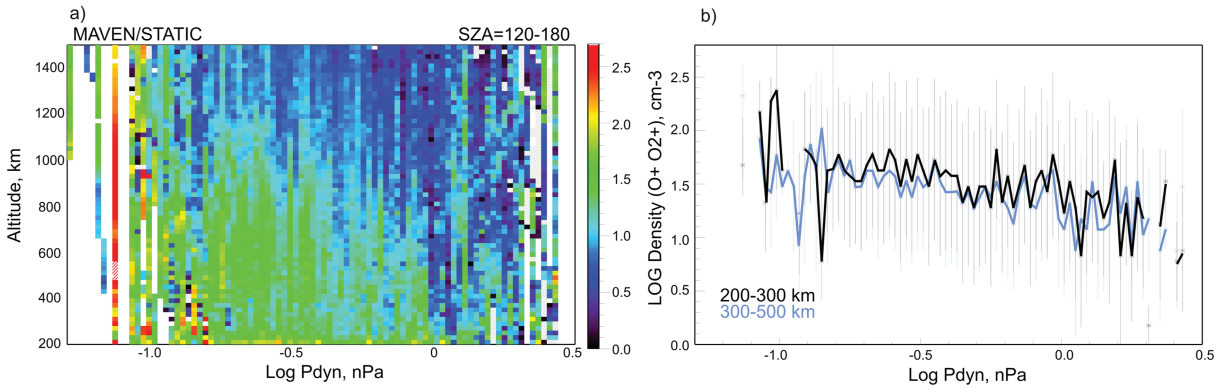

Figure 12. (a) Map of the oxygen ion number density in the ionosphere at SZA = 120–180° as a function of the solar wind dynamic pressure at different altitudes. (b) Density as a function of P_{dyn} at different altitudes.

Figure 5 shows a map of the density at SZA = 60–70° as a function of the cross-flow component of the IMF. The ionosphere is depleted and more patches of planetary plasma are emerging at high altitudes with increasing $B_{\perp}$.

Figure 6 compares the density profiles in the E^{+} and E^{-} hemispheres, respectively. At altitudes above ~300–400 km the density in the E^{-} hemisphere is about 3 times higher than in the opposite hemisphere (see also Dubinin et al., 2018).

Figures 7a and 7b show maps of the ion $(O^{+} + O_2^{+})$ and the proton number densities at different altitudes at SZA = 60–70° as a function of the EUV flux, respectively. Comparing these maps we observe a rather smooth expansion of the ionosphere with increase of the EUV flux from 0.02 to 0.075 W/m^2 implying that the size of the ionospheric obstacle is determined not only by the dynamic pressure of the solar wind but also by the solar irradiance. At higher values of the EUV flux and altitudes below ~500 km the ionospheric density increases. Although at higher altitudes the data are very scarce, we can see here the opposite trend of the ionosphere shrinking. Note that a rise of solar EUV flux is also accompanied by a growth of the proton density in the magnetosheath (Figure 7b) and, correspondingly, by an increase of the dynamic pressure that can result in a contraction of the ionosphere.

Figures 8a and 8b show typical examples of the density for the different EUV conditions. The upper boundary of the ionosphere generally goes upward with increase of the solar irradiance.

It was shown above that the ion density in the topside ionosphere is very responsive to the presence of the crustal magnetic fields. Although solar wind can significantly deform these fields it is useful to look how the ion number density in the ionosphere and the proton density in the sheath vary with the model crustal field. Figure 9a depicts a map of the ion $(O^{+} + O_2^{+})$ number density at different altitudes at SZA = 60–70°

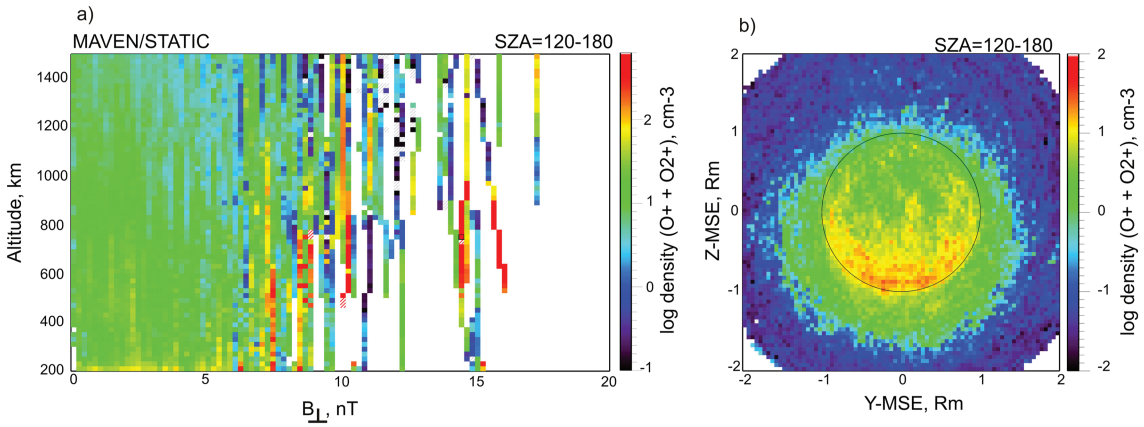

Figure 13. (a) Map of the oxygen ion number density in the ionosphere at SZA = 120–180° as a function of the cross-flow component of the IMF. (b) Map of the density in the *YZ*-MSE plane for the data obtained at SZA = 120–180°.

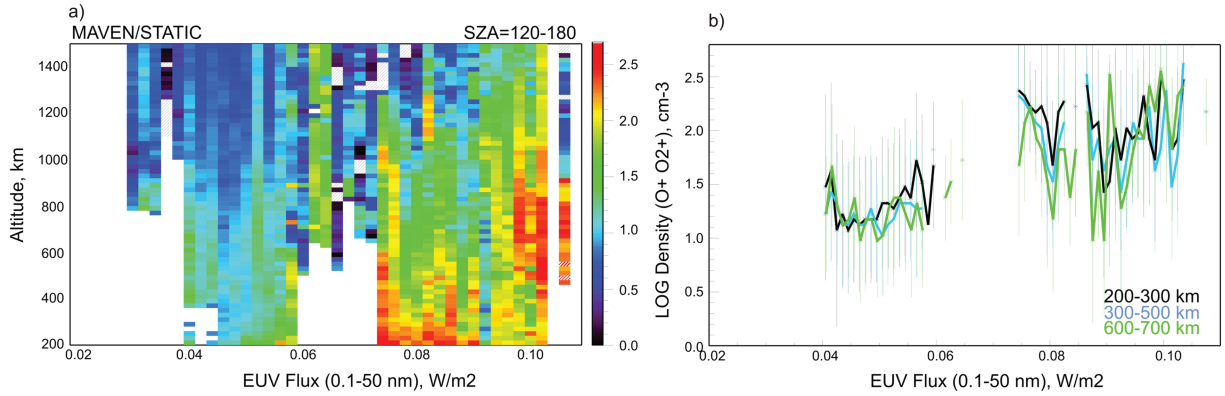

Figure 14. (a) Map of the oxygen ion number density in the ionosphere at SZA = 120–180° as a function of the EUV flux. (b) Density as a function of EUV at different altitudes.

as a function of the crustal magnetic field value at the point of the MAVEN measurements taken from the Cain' model (Cain et al., 2003). It is observed that the density in the ionosphere rises with increase of the magnetic field strength. The effect of crustal magnetic field enhances with altitude. This is clearly seen in Figure 9c, which shows dependences of the density on the field value at the different altitudes. This is in agreement with the MARSIS observations on the Mars Express spacecraft which has no a magnetometer (Dubinin et al., 2016).

However, relations between the ionospheric densities and the actual magnetic field measured by MAVEN occur very different. A map of the ion number density as a function of the in situ measured magnetic field strength does not reveal a drop at low field values (Figure 9b). In contrast, the ionospheric density increases at small field magnitudes (Figure 9c). Such a different behavior is probably related to the fact that besides the crustal field the draping IMF, which is excluded in Figures 9a and 9c, also affects the topside ionosphere. For a better separation of the effects related to the magnetic fields of different origin we have analyzed similar relations for the data obtained in the ionosphere above the northern nonmagnetized lowlands (Lat = 10° ÷ 80°, Long = 160° ÷ 240°), where the magnetic field has primarily IMF origin and for the data in the ionosphere above the southern strongly magnetized areas (Lat = −10° ÷−80°, Long = 160° ÷ 240°) (Figure 10). We observe that the rise of the ion density at low magnetic fields followed by a decrease with increasing magnetic field value as seen in Figures 9b and 9d is associated with the trends, which appear due to the draping IMF component (see Figures 10b and 10d). It is not clear yet whether a sharp increase of the ion density, which appears at $B_t \sim 55$ nT is caused by poor sampling at high values of B_t. In contrast, the density in the areas with strong crustal field sources is almost insensitive to the variations in the field strength.

Figure 11 shows how the ion density in these regions depends on the field geometry. The field geometry is characterized by the inclination angle. An angle of 0° (90°) corresponds to the horizontal (vertical) orientation of the field vector, respectively. In the ionosphere above the southern strongly magnetized areas we do not observe visible variations in the ion density due to the field orientation (Figure 11b). In the areas where the role of the draping IMF is more important, the density sharply decreases for a strongly horizontal (inclination angle ≤20°) field orientation (Figure 11a). It is interesting to note that in the regions with almost vertical field orientation the ion density is almost the same as in the corresponding areas of the southern hemisphere.

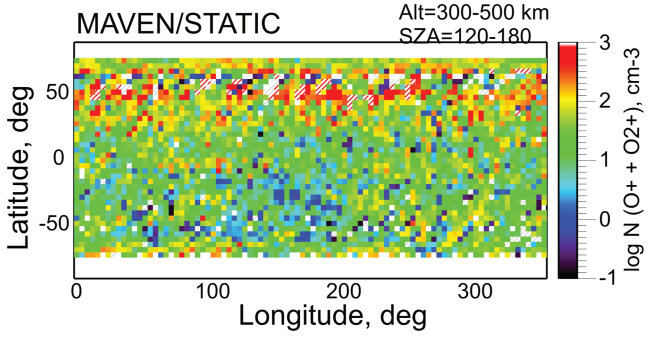

Figure 15. Map of the ion number density at the nightside at altitudes of 300–500 km plotted in areographic coordinates.

2.3. Nightside Ionosphere

For better statistics we consider a broad range (120–180°) of the SZAs. Figure 12 shows how the density at the nightside varies with the solar wind dynamic pressure. Similar to the variations at the dayside, the ion density decreases with rise of the pressure. At $P_{dyn} \geq$ 1–2 nPa the nightside ionosphere becomes very depleted a contains a lot of patches. The dependence on altitude becomes very weak.

Variations caused by the changes in the $B_\perp$ in solar wind bring out a different behavior as compared to the dayside ionosphere (Figure 13a). Although the data at high $B_\perp$ are scarce the trend of the ionosphere intensification is seen. Influence of the direction of the cross-flow IMF component at the nightside occurs even enhanced. The ionosphere significantly shifts in the $V_{sw} \times B_{IMF}$ direction that is well seen in Figure 13b, which shows a map of the ion density in *YZ*-MSE plane created for the data obtained at SZA = 120–180°.

Solar irradiance occurs to be a strong driver for the nightside ionosphere (Figure 14). Here we have a better sampling at high EUV fluxes than at SZA = 60–70° and observe an increase in the density by a factor of 10 when the EUV flux rises only by a factor of 2.

The local magnetic field strongly affects the nightside ionosphere too. Figure 15 presents the ion density in the altitude range of 300–500 km as a function of the areographic coordinates. Contrary to the observations on the dayside, the nightside ionosphere in the southern hemisphere filled by strong crustal magnetic field sources, occurs significantly depleted as compared to the northern hemisphere in which the contribution of the draping field component dominates. A more severe depletion is observed in the region of the strongest crustal fields (compare with Figures 2c and 2d). At midlatitudes in the northern hemisphere the density is 3–4 times higher than in the southern regions. In the regions with strong crustal fields the density rises with an increase of the magnetic field inclination angle implying a possible downward motion of plasma from the dayside that is consistent with the MEX observations (Dubinin et al., 2016) and the additional ionization by the field-aligned suprathermal electrons (Lillis et al., 2018).

3. Discussion

The observations made by the MAVEN spacecraft in the topside (≥200 km) ionosphere of Mars show that this region is very responsive to the variations of the external (solar EUV flux, solar wind, and IMF) and internal (the crustal magnetic field) drivers. At stable conditions in the solar wind the ionosphere broadens with the growth of the solar irradiance. For example, the altitude of the upper boundary of the ionosphere at SZA = 60–70° increases almost linearly from 500 to 1,000 km when the EUV flux increases from 0.03 to 0.06 W/m^2. The observed variations in the topside ionosphere caused by solar EUV flux are in general agreement with the data obtained by Mars Express (Dubinin, Fraenz, Pätzold, Andrews, et al., 2017) although a lack of measurements performed by MAVEN at the dayside at EUV fluxes higher than $\sim$ 0.08 W/m^2 limit the comparison and the extrapolation of the trends. Large variations in the size of the ionospheric obstacle can even lead to the noticeable motions of the bow shock (Hall et al., 2016). The ionosphere expansion with an increase of the EUV flux is also accompanied by enhanced transterminator fluxes of ionospheric ions and their losses (Fraenz et al., 2015; Dubinin, Fraenz, Pätzold, Andrews, et al., 2017; Dubinin, Fraenz, Pätzold, McFadden, Halekas, et al., 2017). Similar variability with solar EUV flux was observed on Venus (Bauer & Taylor, 1981).

The measurements at the nightside show an increase in the density up to a factor of 10 during the times when the EUV flux in the rage of 0.1–50 nm is higher than ~0.08 W/m^2. Such a considerable growth implies that the solar irradiance is the crucial agent for the ion losses. It is worth noting that the nightside ionosphere measurements on Venus also show a strong variability related with the Sun activity. One order of magnitude higher densities were measured by the PVO spacecraft at solar maximum as compared to the measurements by Venera-9,10 at solar minimum (Knudsen et al., 1986).

Large-amplitude motions of the Martian ionosphere occur with variations in the dynamic pressure in the solar wind. The ionosphere contracts to altitudes of $\sim$ 400 km (SZA = 60–70°) during strong events and inflates to altitudes >1,000 km at $P_{dyn} \sim 0.05$ nPa. The absence of the ionospheric compression at low altitudes with increase of P_{dyn} raises the question about the fate of the depleted ionosphere at higher altitudes. A paradox is that, on the one hand, a decrease of the ion fluxes in the tail at high values of the dynamic pressure is observed (Dubinin, Fraenz, Pätzold, McFadden, Mahaffy, et al., 2017; Ramstad et al., 2015). On the other hand, a strong shrinkage of the ionosphere without a noticeable compression implies a loss of a significant portion of the ionospheric plasma. Similar response of the dayside ionosphere was observed on Venus. The measurements made by PVO have shown that the ionopause expands and contracts from ~400 km to over ~1,000 km with changes in solar wind pressure (Brace et al., 1980).

The contraction of the ionosphere propagates also to the nightside. At $P_{dyn} \geq$ 1–2 nPa the nightside ionosphere becomes very fragmented and depleted. A similar behavior of the ionosphere is exposed with

variations of the cross-flow component of the IMF suggesting an important role of the draping IMF in the transport mechanisms.

The upper dayside ionosphere at altitudes of more than 300–400 km occurs also sensitive to the direction of the motional electric field in the solar wind. In the E^- hemisphere in which the motional electric field is pointed toward the Mars-Sun axis the density is higher and the ionosphere expands to higher altitudes. The asymmetry with respect to the $V_{sw} \times B_{IMF}$ direction strongly enhances at the nightside.

The topside ionosphere above the magnetized areas in the southern hemisphere and above the northern nonmagnetized lowlands is also very different. The crustal magnetic field strongly reduces the mobility of ions and electrons making them less exposed to the transport processes (see also Dubinin et al., 2016). As a result, the upper boundary of the ionosphere above the regions with crustal magnetization at the dayside rises and produces the ionospheric bulge (Brain et al., 2005; Dubinin et al., 2008). This difference in altitude of the boundary above the different regions reaches values of 200–300 km. The crustal field also protects the nightside ionosphere from being filled by plasma transported from the dayside. The relations between the ion densities and the values of the model crustal field observed at the dayside by MAVEN are similar to the ones obtained from the Mars Express observations (Andrews et al., 2013; Dubinin et al., 2016)—with density depletions above low magnetic field regions. There was no a magnetometer on Mars Express and therefore relations between the actual magnetic field and the ionospheric density could not be studied before the MAVEN arrival to Mars. The MAVEN in situ observations show that these relations are very different and do not reveal a drop at low magnetic fields.

Effects of the draping component of the magnetic field of the IMF origin were also studied. We have shown that the draping IMF penetrates deeply into the ionosphere and actively influences its structure. Weak fields and, correspondingly, weak magnetic field forces only slightly affect the ionosphere. With increase of the induced magnetic field strength the transport motions driven by the magnetic field pressure and field tensions seem to be intensified and we observe that the local ion densities considerably decrease. The reduction in the ion density at $h \sim$ 300–600 km at $B_t \sim$ 40–50 nT reaches a factor of more than 10. This suggests an enhanced transport of the plasma for the horizontal field orientation, when the magnetic field forces are maximized. In the ionosphere above the regions with strong crustal magnetic fields the ion density is almost insensitive to the field strength and its direction.

A comparison between the nightside ionospheres in the northern and the southern hemispheres shows a different trend. The ion density in the ionosphere above the northern lowlands is higher than in the southern hemisphere. Such a tendency indicates that plasma transport from the dayside is the main source of the nightside ionosphere. In the regions void of strong crustal sources transport processes are more effective. In the nightside ionosphere above large crustal fields the density rises with an increase of the inclination angle suggesting an easier access of plasma to low altitudes and the ionization by the field-aligned magnetospheric electrons.

In conclusion, we note that constant variations in the solar EUV flux, the solar wind dynamic pressure, the IMF value and the field orientation, and the variations of the crustal magnetic field due to Mars rotation lead to a continuous large-amplitude motions of the ionosphere that must have a strong impact on the dynamics of the ionospheric losses.

Acknowledgments
The MAVEN project is supported by NASA through the Mars Exploration Program. MAVEN data are publicly available through the Planetary Data System. Authors E. D. and M. P. wish to acknowledge support from DFG for supporting this work by Grant PA 525/14-1. Authors E. D. and M. F. wish to acknowledge support from DLR by Grant 50QM1703. O. V. and L. Z. wish to acknowledge support from the Russian Science Foundation by Grant 16-42-01 103.

References

Açuna, M. H., Connerney, J. E. P., Ness, N. F., Lin, R. P., Mitchell, D., Carlson, C. W., et al. (1999). Global distribution of crustal magnetism discovered by Mars Global Surveyor MAG/ER experiment. *Science*, *284*, 790–793. https://doi.org/10.1126/science.284.5415.790

Andrews, D. J., Opgenoorth, H. J., Edberg, N. J. T., André, M., Fränz, M., Dubinin, E., et al. (2013). Determination of local plasma densities with the MARSIS radar: Asymmetries in the high-altitude Martian ionosphere. *Journal of Geophysical Research*, *118*, 6188–6196. https://doi.org/10.1002/jgra.50593

Bauer, S., & Taylor, H. (1981). Modulation of Venus ion densities associated with solar variations. *Geophysical Research Letters*, *8*, 840–842. https://doi.org/10.1029/GL008i007p00840

Benna, M., Mahaffy, P. R., Grebowsky, J. M., Fox, J. L., Yelle, R. V., & Jakosky, B. M. (2015). First measurements of composition and dynamics of the Martian ionosphere by MAVEN's Neutral Gas and Ion Mass Spectrometer. *Geophysical Research Letters*, *42*, 8958–8965. https://doi.org/10.1002/2015GL066146

Bougher, S. W., B. Jakosky, J. Halekas, J. Grebowsky, J. Luhmann, P. Mahaffy, et al. (2015). Early MAVEN dip deep campaign reveals thermosphere and ionosphere variability. *Science*, *350*, 1-7. https://doi.org/10.1126/science.aad0459

Brace, L. H., Theis, R. F., Hoegy, W. R., Wolfe, J. H., Mihalov, J. D., Russell, C. T., et al. (1980). The dynamic behavior of the Venus ionosphere in response to solar wind interactions. *Journal of Geophysical Research*, *85*(A13), 7663–7678. https://doi.org/10.1029/JA085iA13p07663

Brain, D., Halekas, J. S., Lillis, R., Mitchell, D. L., Lin, R. P., & Crider, D. H. (2005). Variability of the altitude of the Martian sheath. *Geophysical Research Letters*, *321*, L18203. https://doi.org/10.1029/2005GL023126

Cain, J. C., Ferguson, B. B., & Mozzoni, D. (2003). An $n = 90$ internal potential function of the Martian crustal magnetic field. *Journal of Geophysical Research*, *108*(E2), 5008. https://doi.org/10.1029/2000JE001487

Connerney, J. E. P., Açuna, M. H., Ness, N. F., Kletetschka, G., Mitchell, D. L., Lin, R. P., & Reme, H. (2005). Tectonic implications of Mars crustal magnetism. *Proceedings of the National Academy of Sciences of the United States of America*, *102*(42), 14,970–14,975. https://doi.org/10.1073/pnas.0507469102

Connerney, J. E. P., Espley, J., DiBraccio, G. A., Gruesbeck, J. R., Oliversen, R. J., Mitchell, D. L., et al. (2015). First results of the magnetic field investigation. *Geophysical Research Letters*, *42*, 8819–8827. https://doi.org/10.1002/2015GL065366

Connerney, J. E. P., Espley, J., Lawton, P., Murphy, S., Odom, J., Oliversen, R., & Sheppard, D. (2015). The MAVEN magnetic field investigation. *Space Science Reviews*, *195*(1-4), 257–291. https://doi.org/10.1007/s11214-015-0169-4

Dubinin, E., Chanteur, G., Fraenz, M., Modolo, R., Woch, J., Roussas, E., et al. (2008). Asymmetry of plasma fluxes at Mars: ASPERA-3 observations and hybrid simulations. *Planetary and Space Science*, *56*, 832–835. https://doi.org/10.1016/j.pss.2007.12.006169

Dubinin, E., Fraenz, M., Andrews, D., & Morgan, D. (2016). Martian ionosphere observed by Mars Express: 1. Influence of the crustal magnetic fields. *Planetary and Space Science*, *124*, 62–75. https://doi.org/10.1016/j.pss.2016.02.004

Dubinin, E., Fraenz, M., Pätzold, M., Andrews, D., Vaisberg, O., Zelenyi, L., & Barabash, S. (2017). Martian ionosphere observed by Mars Express: 2. Influence of solar irradiance on upper ionosphere and escape fluxes. *Planetary and Space Science*, *145*, 1–8. https://doi.org/10.1016/j.pss.2017.07.002

Dubinin, E., Fraenz, M., Pätzold, M., McFadden, J., Halekas, J. S., Connerney, J. E. P., et al. (2018). Martian ionosphere observed by MAVEN. 3. Influence of solar wind and IMF on upper ionosphere. *Planetary and Space Science*, *160*, 56–65. https://doi.org/10.1016/j.pss.2018.03.016

Dubinin, E., Fraenz, M., Pätzold, M., McFadden, J., Halekas, J. S., DiBraccio, G. A., et al. (2017). The effect of solar wind variations on the escape of oxygen ions from Mars through different channels: MAVEN observations. *Journal of Geophysical Research*, *122*, 11,285–11,301. https://doi.org/10.1002/2017JA024741

Dubinin, E., Fraenz, M., Pätzold, M., McFadden, J., Mahaffy, P. R., Eparvier, F., et al. (2017). Effects of solar irradiance on the upper ionosphere and oxygen ion escape at Mars: MAVEN observations. *Journal of Geophysical Research: Space Physics*, *122*, 7142–7152. https://doi.org/10.1002/2017JA024126

Eparvier, F. G., Chamberlin, P. C., Woods, T. N., & Thiemann, E. M. B. (2015). The solar extreme ultraviolet monitor for MAVEN. *Space Science Reviews*, *195*, 293–301. https://doi.org/10.1007/s11214-015-0195-2

Ergun, R. E., Morooka, M. W., Andersson, L. A., Fowler, C. M., Delory, G. T., Andrews, D. J., et al. (2015). Dayside electron temperature and density profiles at Mars: First results from the MAVEN Langmuir probe and waves instrument. *Geophysical Research Letters*, *42*, 8846–8853. https://doi.org/10.1002/2015GL065280

Fox, J. L. (2004). Response of the Martian thermosphere/ionosphere to enhanced fluxes of solarsoft X rays. *Journal of Geophysical Research*, *109*, A11310. https://doi.org/10.1029/2004JA010380

Fox, J. L., Johnson, A. S., Ard, S. G., Shuman, N. S., & Viggiano, A. A. (2017). Photochemical determination of O densities in the Martian thermosphere: Effect of a revised rate coefficient. *Geophysical Research Letters*, *44*, 8099–8106. https://doi.org/10.1002/2017GL074562

Fraenz, M., Dubinin, E., Andrews, D., Nilsson, H., & Fedorov, A. (2015). Cold ion escape from the Martian ionosphere. *Planetary and Space Science*, *119*(15), 92–102. https://doi.org/10.1016/j.pss.2015.07.012

Fraenz, M., Dubinin, E., Nielsen, E., Woch, J., Barabash, S., Lundin, R., & Fedorov, A. (2010). Transterminator ion flow in the Martian ionosphere. *Planetary and Space Science*, *58*, 1442–1454. https://doi.org/10.1016/j.pss.2010.06.009

Girazian, Z., Mahaffy, P., Lillis, R., Benna, M., Elrod, M., & Jakosky, B. (2017). Nightside ionosphere of Mars: Composition, vertical structure and variability. *Journal of Geophysical Research*, *122*, 4712–4725. https://doi.org/10.1002/2016/JA023508

Gurnett, D., Huff, R. L., Morgan, D. D., Persoon, A. M., Averkamp, T. F., et al. (2008). An overview of radar soundings of the Martian ionosphere from the Mars Express spacecraft. *Advances in Space Research*, *41*, 1335–1346. https://doi.org/10.1016/j.asr.2007.01.062

Gurnett, D., Kirchner, D. L., Huff, R. L., Morgan, D. D., Persoon, A. M., Averkamp, T. F., et al. (2005). Radar soundings of the ionosphere of Mars. *Science*, *310*, 1929–1933.

Halekas, J., Taylor, E., Dalton, G., Johnson, G., Curtis, D., McFadden, J., et al. (2015). The solar wind ion analyzer for MAVEN. *Space Science Reviews*, *195*, 125–151. https://doi.org/10.1007/s11214-013-0029-z

Hall, B. E. S., Lester, M., Sánchez-Cano, B., Nichols, J. D., Andrews, D. J., Edberg, N. J. T., et al. et al. (2016). Annual variations in the Martian bow shock location as observed by the Mars Express mission. *Journal of Geophysical Research: Space Physics*, *121*, 11,474–11,494. https://doi.org/10.1002/2016JA023316

Hanson, W. B., Satani, S., & Zuccaro, D. R. (1977). The Martian ionosphere as observed by the Viking retarding potential analyzers. *Journal of Geophysical Research*, *82*, 4351–4363. https://doi.org/10.1029/JS082i028p04351

Hinson, D., Simpson, R. A., Twicken, J. D., Tyler, G. L., & Flasar, F. M. (1999). Initial results from radio occultation measurements with Mars Global Surveyor. *Journal of Geophysical Research*, *104*, 26,997–27,012.

Jakosky, B. M., Lin, R. P., Grebowsky, J. M., Luhmann, J. G., Mitchell, D. F., Beutelschies, G., et al. (2015). The Mars Atmosphere and Volatile Evolution (MAVEN) mission. *Space Science Reviews*, *195*(1-4), 3–48. https://doi.org/10.1007/s11214-015-0139-x

Kliore, A. (1992). Radio occultation observations of the ionospheres of Mars and Venus. In J. Luhmann, M. Tatrallyay, & R. Pepin (Eds.), *Venus and Mars: Atmospheres, Ionospheres and Solar Wind Interactions, Geophysical Monograph Series* (Vol. *66*, pp. 265–276). Washington, DC: AGU. http://doi.org/10.1029/GM066p0265

Kliore, A., Cain, D. L., Levy, G. S., Eshleman, V. R., Fjeldbo, G., & Drake, F. D. (1965). Occultation experiment: Results of the first direct measurement of Mars atmosphere and ionosphere. *Science*, *149*, 1243–1248.

Knudsen, W. C., Miller, K., & Spenner, K. (1986). Median density altitude profiles of the major ions in the central nightside Venus ionosphere. *Journal of Geophysical Research*, *91*, 936–950.

Kopf, A., Gurnett, D. A., Morgan, D. D., & Kirchner, D. L. (2008). Transient layers in the topside ionosphere of Mars. *Geophysical Research Letters*, *35*, L17102. https://doi.org/10.1029/2008GL034948

Lee, C. O., Jakosky, B. M., Luhmann, J. G., Brain, D. A., Mays, M. L., Hassler, D. M., et al. (2018). Observations and impacts of the 10 September 2017 solar events at Mars: An overview and synthesis of the initial results. *Geophysical Research Letters*, *45*, 8871–8885. https://doi.org/10.1029/2018GL079162

Lillis, R., Mitchel, D., Steckiewicz, M., Brain, D., Xu, S., Weber, T., et al. (2018). Ionizing electrons on the nightside ionosphere: Structure and variability. *Journal of Geophysical Research: Space Physics*, *123*, 4349–4363. https://doi.org/10.1029/2017JA025151

Ma, Y., Fang, X., Halekas, J. S., Xu, S., Russell, C. T., Luhmann, J. G., et al. (2018). The impact and solar wind proxy of the 2017 September ICME event at Mars. *Geophysical Research Letters*, *45*, 7248–7256. https://doi.org/10.1029/2018GL077707

McFadden, J. P., Kortmann, O., Curtis, D., Dalton, G., Johnson, G., Abiad, R., et al. (2015). MAVEN SupraThermal and Thermal Ion Compostion (STATIC) instrument. *Space Science Reviews*, *195*, 199–256. https://doi.org/10.1007/s11214-015-0175-6

Mendillo, M., Marusiak, A., Withers, P., Morgan, D., & Gurnett, D. (2013). A new semi-empirical model of the peak electron density of the Martian ionosphere. *Geophysical Research Letters*, *40*, 5361–5365. https://doi.org/10.1002/2013GL057631

Mendillo, M., Narvaez, C., Vogt, M. F., Mayyasi, M., Forbes, J., Galand, M., et al. (2017). Sources of ionospheric variability at Mars. *Journal of Geophysical Research: Space Physics*, *122*, 9670–9684. https://doi.org/10.1002/2017JA024366

Mendillo, M., Trovato, J., Narvaez, C., Mayassi, M., Moore, L., Vogt, M. F., et al. (2016). Comparative aeronomy: Molecular ionospheres at Earth and Mars. *Journal of Geophysical Research*, *121*, 10,269–10,288. https://doi.org/10.1002/2016JA023097

Mendillo, M., Withers, P., Hinson, D., Rishbeth, H., & Reinisch, B. (2006). Effects of solar flares on the ionosphere of Mars. *Science*, *311*, 1135–1138. https://doi.org/10.1126/science.112209

Pätzold, M., Husler, B., Tyler, G. L., Andert, T., Asmar, S. W., Bird, M. K., et al. (2016). Mars Express 10 years at Mars: observations by the Mars express radio science experiment (MaRS). *Planetary and Space Science*, *127*, 44–90. https://doi.org/10.1016/j.pss.2016.02.013

Pätzold, M., Tellmann, S., Häusler, B., Hinson, D., Schaa, R., & Tyler, G. L. (2005). A sporadic third layer in the ionosphere of Mars. *Science*, *5749*, 837–839.

Pätzold, M., et al. (2009). in Mars express, ed. by K. Fletcher, 217-245, ESA Communication Production Office, Noordwijk.

Peter, K., Pätzold, M., Molina-Cuberos, G., Witasse, O., Gonzales-Galindo, F., Withers, P., Bird, M. K., Häusler, B., Hinson, D. P., Tellmann, S., & Tyler, G. L. (2014). The dayside ionospheres of Mars and Venus: Comparing a one-dimensional photochemical model with MaRS (Mars Express) and VeRa (Venus Express) observations. *Icarus*, *233*, 66–82. https://doi.org/10.1016/j.icarus.2014.01.028

Phillips, J. L., Luhmann, J. G., & Russell, C. T. (1985). Dependence of Venus ionopause altitude and ionospheric magnetic field on solar wind dynamic pressure. *Advances in Space Research*, *5*(9), 173–176.

Ramstad, R., Barabash, S., Futaana, Y., Nilsson, H., Wang, X. D., & Holmström, M. (2015). The Martian atmospheric ion escape rate dependence on solar wind and solar EUV conditions: I. Seven years of Mars Express observations. *Journal of Geophysical Research: Planets*, *120*, 1298–1309. https://doi.org/10.1002/2015JE004816

Sanchez-Cano, B., Lester, M., Witasse, O., Milan, S. E., Hall, B. E. S., Blelly, P.-L., et al. (2015). Evidence of scale height variations in the Martian ionosphere over the solar cycle. *Journal of Geophysical Research: Space Physics*, *120*, 10,913–10,925. https://doi.org/10.1002/2015JA021949

Sanchez-Cano, B., Lester, M., Witasse, O., Milan, S. E., Hall, B. E. S., Cartacci, M., et al. (2016). Solar cycle variations in the ionosphere of Mars as seen by multiple Mars Express data sets. *Journal of Geophysical Research: Space Physics*, *121*, 2547–2568. https://doi.org/10.1002/2015JA022281

Schunk, R. W., & Nagy, A. F. (2009). Ionospheres, (2nd ed.). Cambridge, UK: Cambridge Univ. Press.

Venkateswara Rao, N., Balan, N., & Patra, A. K. (2014). Solar rotation effects on the Martian ionosphere. *Journal of Geophysical Research: Space Physics*, *119*, 6612–6622. https://doi.org/10.1002/2014JA019894

Withers, P., & Mendillo, M. (2005). Response of peak electron densities in the Martian ionosphere to day-to-day changes in solar flux due to solar rotation. *Planetary and Space Science*, *53*, 1401–1418. https://doi.org/10.1016/j.pss.2005.07.010

Withers, P., Morgan, D. D., & Gurnett, D. A. (2015). Variations in peak electron densities in the ionosphere of Mars over a full solar cycle. *Icarus*, *251*, 5–11. https://doi.org/10.1016/j.icarus.2014.08.008